SAKARYA ÜNİVERSİTESİ
FEN BİLİMLERİ ENSTİTÜSÜ DERGİSİ

Sakarya University Journal of Science
SAUJS

e-ISSN 2147-835X | Period Bimonthly | Founded: 1997 | Publisher Sakarya University |
http://www.saujs.sakarya.edu.tr/en/

Title: Comparison of Two Different Circular Diaphragm Models with Central Mass for MEMS Based FPI Pressure Sensor Performance Based on Sensitivity and Frequency Response

Authors: Fikret YILDIZ

Recieved: 2020-05-15 16:28:37

Accepted: 2021-04-01 11:55:19

Article Type: Research Article

Volume: 25
Issue: 3
Month: June
Year: 2021
Pages: 619-628

How to cite
Fikret YILDIZ; (2021), Comparison of Two Different Circular Diaphragm Models with Central Mass for MEMS Based FPI Pressure Sensor Performance Based on Sensitivity and Frequency Response. Sakarya University Journal of Science, 25(3), 619-628, DOI: https://doi.org/10.16984/saufenbilder.737982
Access link
http://www.saujs.sakarya.edu.tr/en/pub/issue/62736/737982

Sakarya University Journal of Science 25(3), 619-628, 2021

Comparison of Two Different Circular Diaphragm Models with Central Mass for MEMS Based FPI Pressure Sensor Performance Based on Sensitivity and Frequency Response

Fikret YILDIZ[*1]

Abstract

The sensitivity and the fundamental frequency of circular membrane with a central mass (embossment) were analytically evaluated for Fabry- Pérot interferometers (FPI) based pressure sensor. Two different previously developed model (named as M1 and M2, respectively in this study), which includes a diaphragm with center embossment, were considered to obtain results and performance of models were compared. Thickness of diaphragms were 5 µm and 10 µm with the radius of 300 µm, 500 µm,600 µm and 700 µm, respectively. According to the results, it was noted that diaphragm considering M1 model shows higher sensitivity and displacement compared to diaphragm considering M2 model. 155.15-102.87 nm/kPa and 149.5-39.7 nm/kPa sensitivity range were calculated for the diaphragm based on the M1and M2 model, respectively when 300 µm in radius and 5 µm thick diaphragm was used. Moreover, frequency response of diaphragm considering two different model is slightly different for thinner embossment; however, same frequency response was calculated for thicker embossment. For example, frequency range of 700 µm in radius and 10 µm was changes between 42-22.7 kHz and 42.2-22.7 kHz when M1 and M2 model was considered. It was understand that compared with the conventional circular diaphragm (CD) model, non-uniform diaphragm with a central mass provides more geometrical parameters to tune the device performance (sensitivity) and it provides design flexibility on the sensor structure.

Keywords: central embossment, FPI pressure sensor, MEMS, sensitivity analyze

1. INTRODUCTION

Pressure is a fundamental parameter and significance for different applications [1-4]. It has studied intensively for years [5]. Pressure sensors based on piezo resistive/piezoelectric effects have dominantly used in this field. However, electromagnetic interference still is an issue such type of devices [6,7]. Fiber optic pressure sensors are the alternative to the conventional piezo resistive/piezoelectric based sensors [8]. Some of them are Mach-Zehnder interferometers and Fabry-Pérot interferometers (FPI) [9-14]. FPI-

[*]Corresponding author: fikretyildiz@hakkari.edu.tr
[1]Hakkari University, Faculty of Engineering, Electrical and Electronics Engineering Department, 30000, Hakkari,Turkey
ORCID: https://orcid.org/0000-0003-4846-3998

based sensors have various superiorities among the other fiber optic sensors [14-17]. Reflecting parallel mirrors separated by a gap (cavity) are the main component of the FPI-based pressure sensor [3]. Extrinsic cavity with a diaphragm is commonly used for variety applications [5], [18,19]. An extrinsic Fabry-Pérot interferometer is placed between a fiber end face and a reflective membrane [20]. Thus, the choice of diaphragm material and geometry is a key factor for pressure sensor design [21]. Some of the studies related to MEMS based FPI pressure sensors are summarized below.

Rectangular, square or circular shape flat diaphragm have extensively used in the MEMS based pressure sensor technology. In one study, the design guidelines of pressure sensors with a square shape diaphragm have presented by considering the relationships between diaphragm thickness, side length, sensitivity and resonant frequency [22]. Another study of different research group used a piezoresistive pressure sensor with polysilicon piezoresistors and a square shape diaphragm for high temperature applications in the desired operation range (0–30 Bar). Fabricated sensor results show good sensitivity and linearity [23]. In the different work, a micro piezoresistive pressure sensor was designed, fabricated using wet etching technology and tested for Tire Pressure Measurement System (TPMS) [24]. Another previous study designed, fabricated, and tested the micro pressure sensor with a square diagram made of silicon and bossed diaphragm. 11.098 μV/V/Pa sensitivity was measured in the operating range of 500 Pa and it was confirmed that the sensor enables to measure the absolute micro pressure lower than 500 Pa [25]. More studies are available and can be found in literature [26].

Square diaphragm as a pressure sensor commonly used due to better sensitivity than rectangular diaphragm or circular diaphragm under same conditions [23]. However, advantages of compatibility with standard fiber components make circular geometries more use in literature for numerical and analytical modeling [27-30]. Moreover, the sensitivity and the frequency response of the circular diaphragm are tuned by less geometric parameters compared to square or rectangular shape geometry [22-28]. However, one of the disadvantage of flat diaphragms is pressure induced large deflections and thus, undesired volatility effects to the output of the sensor [21]. Hence, many innovative sensor designs have been widely explored in the past decades with the aim of fabrication of high performance pressure sensors. Placing a center mass on diaphragm is an effective method to improve sensor characteristics by increase the stiffness of the diaphragm and reduce the nonlinear effects [21].

In this paper, two different model of center-embossed circular diaphragm, which were previously developed and available in literature [26,33], were used to determine performance and behaviors of the circular diaphragm with a center embossment (mass). These two models explained in the following section of study. The sensitivity and frequency response as a function of embossment thickness and radius at a given pressure were obtained. Then performance of pressure sensors based on embossed diaphragm results were compared and discussed considering the two different circular diaphragm models with a central mass.

2. SENSOR DESIGN

In general, a fiber optic EFPI (Extrinsic Fabry-Pérot Interferometer) system composed of a sensor probe, a fiber optic coupler, a light source, and a detector [31,32] as illustrated in Figure 1. Membrane is the main part of the sensing probe, which sense the acoustic signal. In this system, the light emitted by the source passing through the fiber optic coupler is reflected from two different surface: fiber optic coupler and diaphragm. Detection of incoming pressure waves is measured by comparison of light intensity of reflected light from first and second surface (membrane). The membrane structure is deformed under pressure and, thus, change the cavity length, which results in the phase differences between collected light from the consecutive surfaces [28,31]. Therefore, the membrane deflection due to the acoustic pressure determines the performance of FPI system in

terms of the sensitivity and linear range. Frequency response also an important parameter to evaluate sensor characteristic. Two of FPI sensor designs, (a) conventional circular diaphragm and (b) center embossment diaphragm, are illustrated in Figure 2.

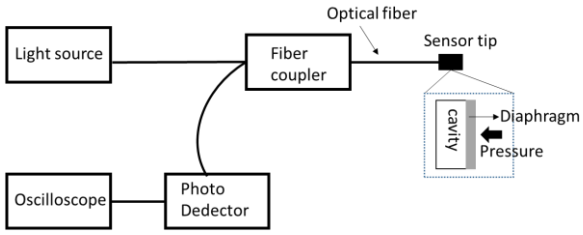

Figure 1 Schematic of a FPI pressure sensor components

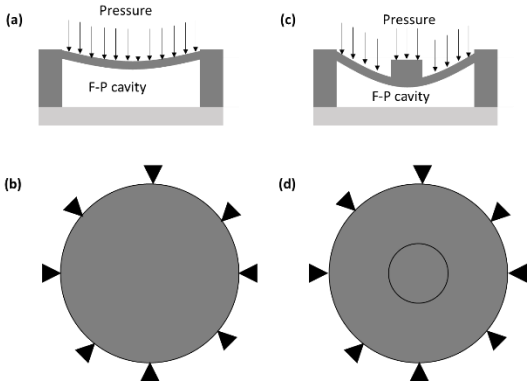

Figure 2 Schematic of FPI pressure sensor. (a) Cross-sectional and (b) top view of conventional circular diaphragm sensor. (c) Cross-sectional and (d) top view of embossed diaphragm

Analysis of FPI pressure sensor, thus, can be initiated by considering its diaphragm geometry. Different kind of diaphragms have been designed in literature [22,23], [27-29]. One approaches is the use of non-uniform membrane by adding a mass on the geometrical center of vibrating membrane [26,33,34]. Under the small deflection approximation, the equation governing deflection, w(r), of a thin flexible circular plate with radius, *R*, under a uniform loading, P, is given as [35-37]

$$\nabla^2 w \nabla^2 D = \mathrm{P} \tag{1}$$

$$D = \frac{Eh^3}{12(1-v^2)} \tag{2}$$

Here, P is the applied pressure, D is the flexural rigidity of the plate, E is the Young's modulus, h is the diaphragm thickness, and ν is the Poisson's ratio. The differential operator (∇) in cylindrical coordinates is given by Eq.3. When substitution Eq.3 into Eq.1 and considering D is constant through the plate, Eq.4 is obtained.

$$\nabla^2 = \frac{\partial}{\partial r^2} + \frac{1}{r^2}\frac{\partial^2}{\partial \emptyset^2} + \frac{1}{r}\frac{\partial}{\partial r} \tag{3}$$

$$\nabla^2 w = \mathrm{P/D}$$

The vertical deflection w (r) is obtained as

$$w(r) = \frac{Pr^4}{64D}\left\{1 - \left(\frac{r}{R}\right)^2\right\}^2 \tag{4}$$

$$w(r=0) = w_{max} = \frac{Pr^4}{64D}$$

Eq.4 describes the deflection of clamped circular diaphragm (CD) (Figure 2 (a-b)). Deflection profile of non-uniform membrane as illustrated in Figure 2 (c-d), can be re-established using above equation of clamped thin circular membrane [33]. In this study, two different model of central embossment membrane were considered for calculation of frequency response and sensitivity.

In the first model named as M1 in this study, deflection of center embossment membrane (Y_0) is analytically expressed as in Eq.5 as described previously in [26]:

$$Y_0 = \frac{A_p a^4 P}{EH^3} \tag{5}$$

$$A_p = \frac{3(1-v^2)}{16}\left(1 - \frac{b^4}{a^4} - 4\frac{b^2}{a^2}\log\frac{a}{b}\right) \quad (6)$$

where H is the thickness of membrane, b is the radius of embossment and a is the radius of membrane.

To obtain simplified analytical model of the center-embossed diaphragm, it is divided into two parts [33], which is named as as M2 in this study. First part is referring to a thin round plates expect that there is a circular hole in the center. Second part defines the circular plates with a sum of thickness of a central mass and diaphragms. More details can be found about analytical model of center-embossed membrane in [33]. Center deflection and structural sensitivity of embossed membrane under constant pressure is expressed as Eq.7-8 [33];

$$w_0 = \left(\frac{[D_0 r_1^4 + D_1(r_0^4 - r_1^4)]}{64 D_0 D_1} + \frac{(D_1 - D_0)(r_0^2 - r_1^2) r_0^2 r_1^2 \ln\frac{r_1}{r_0}}{16 D_0\left[D_1(r_0^2 - r_1^2) + D_0\left(\frac{1-v}{1+v}r_0^2 + r_1^2\right)\right]}\right) P \quad (7)$$

$$S = \frac{w_0}{P} = \frac{[D_0 r_1^4 + D_1(r_0^4 - r_1^4)]}{64 D_0 D_1} + \frac{(D_1 - D_0)(r_0^2 - r_1^2) r_0^2 r_1^2 \ln\frac{r_1}{r_0}}{16 D_0\left[D_1(r_0^2 - r_1^2) + D_0\left(\frac{1-v}{1+v}r_0^2 + r_1^2\right)\right]} \quad (8)$$

where D0 and D1 denote the flexural rigidities of first and second part, respectively, which can be expressed as below and H is the thickness of central mass, r0 is the radius of the membrane and r1 is the radius of embossment.

$$D_0 = \frac{Eh^3}{12(1-v^2)} \; and \quad D_1 = \frac{E(h+H)^3}{12(1-v^2)} \quad (9)$$

When the central embossment ignored, in other word H = 0 or $r_0 = r_1$, sensitivity equals to $r_0/64D_0$ same as the clamped round shape plate [33]. The resonance frequency of a circular and fixed diaphragm is expressed as Eq.10 [38];

$$f = \frac{1}{2\pi}\sqrt{\frac{k_m}{m_m + m_a}} \quad (10)$$

here, k_m is elastic coefficient of the membrane, m_m is mass of the membrane, m_a any additional mass on the surface of the membrane. The elastic coefficient, k_m, of the membrane depends on its shape and can be calculated using Hooke's law, having a circular shaped membrane with a radius of a_m

$$k_m = \frac{188D}{a_m^2} \quad (11)$$

where D is the flexural rigidity of membrane. In this study, FPI diaphragm with a central mass was analytically evaluated using the previously developed two different models and these models are available in literature [26,33]. Sensitivity and frequency response were calculated and results of diaphragm with a central mass considering two different models were compared.

3. RESULTS AND DISCUSSION

Two different model of center-embossed membranes were used to obtain analytical results in terms of sensitivity and frequency response. Displacement profile of first model (M1) is not include effect of embossment thickness [26]. On the other hand, thickness of embossment is considered for analytical results for second model(M2) [33]. Performance of these two model

was evaluated in terms of sensitivity and frequency response of center embossed diaphragm. Moreover, results were also compared with the conventional circular design (CD).

3.1. Frequency Response

Different geometrical values were selected for frequency response analysis; membrane radius (r_0), embossment radius (r_{em}) and thickness of embossment (t_{em}). Calculations were performed for the 5 µm and 10 µm thick membranes, respectively. SiO_2 was selected as diaphragm and embossment material (E=73 GPa, υ=0.17 and ρ=2200 kg/m^3 [39]). The fundamental frequency of diaphragm considering the M1 model and M2 model was calculated using Eq.10 and the results were presented in Table 1. Figure 3 shows the fundamental frequency of diaphragm considering M1 and M2 model as a function of thickness of central embossment (t_{em}) and radius (r_{em}) when the thickness of diaphragm is 5 µm. Maximum thickness of embossment was selected up to 10 times of membrane thickness. Similarly, embossment radius (r_i in Fig.3) was selected as 10%, 30% and 50% of membrane radius. It has been observed that as the embossment thickness increases fundamental frequency of structures as expected based on the Eq.10. Comparatively, the embossment radius has an obviously impact on the fundamental frequency.

Table 1
Frequency (kHz) response of diaphragm considering CD, M1 and M2 model for different membrane thicknesses

r_0 (µm)	**t_m (µm)=5**			**t_m (µm)=10**		
	CD	**M1**	**M2**	**CD**	**M1**	**M2**
		t_{em}=5-50 (µm) r_{em}= r_0 /2 (max.)	**t_{em}=5-50 (µm) r_{em}= r_0 /2 (max.)**		**t_{em}=10-100 (µm) r_{em}= r_0 /2 (max.)**	**t_{em}=10-100 (µm) r_{em}= r_0 /2 (max.)**
300	152.34	114.3-61.7	114.8-61.7	304.67	228.6-123.4	229.5-123.4
500	54.84	41.1-22.2	41.3-22.2	109.68	82.3-44.4	82.6-44.4
600	38.08	28.6-15.4	28.7-15.4	76.17	57.1-30.8	57.4-30.8
700	27.98	21-11.3	21.1-11.3	55.96	42-22.7	42.2-22.7

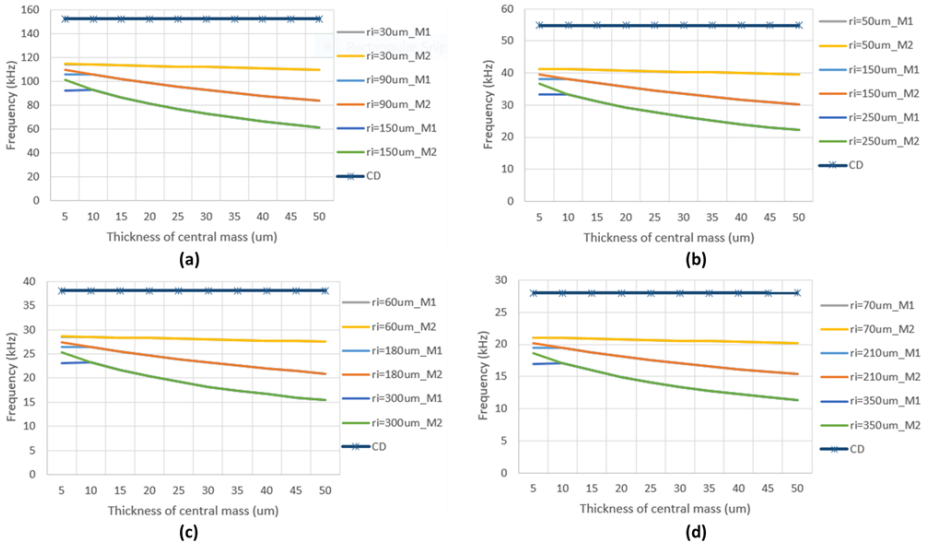

Figure 3 Comparison of frequency response for the diaphragm using M1 and M2 model, respectively. (a) t_m=5 µm and r_0=300 µm, (b) t_m=5 µm and r_0=500 µm,(c) t_m=5 µm and r_0=600 µm and (d) t_m=5 µm and r_0=700 µm

Fundamental frequency results of diaphragm with a central mass was very close when both the M1 and M2 model were considered. It was seen form the Figure 3 that the diaphragm with same

embossment thickness and radius have almost same frequency response when M1 and M2 models were considered separately. For example, fundamental frequency of diaphragm based on M1 and M2 models are 105.9 kHz and 109.9 kHz, respectively with a 5 µm thick embossment and radius of 90 µm (30%xr_0). However, when thicker embossment selected, this differences is vanished as shown in Fig.3. From the Table 1 and Fig.3, the fundamental frequency of CD is constant and higher than M1 model and M2 model. This is the results of increased membrane mass due to embossment as in Eq.10. It can be concluded that pressure sensor diaphragm with a central embossment is suitable for low frequency and wide frequency bandwidth applications compared to CD structure.

3.2. Sensitivity

As mentioned in the design section, the sensitivity, S, of pressure sensor is defined as ratio of center displacement to pressure. To obtain the sensitivity values of diaphragm, first membrane deformation was calculated under acoustic pressure ranging from 1 Pa to 10 kPa [20]. Then, the sensitivities for different cases depending on the embossment thickness and radius were obtained for the CD, M1 and M2 model. The results are listed in Table 2. Figure 4 shows the sensitivity of diaphragm with a thickness of 10 µm. From these results, diaphragm considering M1 model has higher sensitivity than its M2 model based diaphragm counterparts.

Table 2
Sensitivity (nm/kPa) performance of CD, M1 and M2 models for different membrane thicknesses

r_0 (µm)	**t_m (µm)=5**			**t_m (µm)=10**		
	CD	**M1**	**M2**	**CD**	**M1**	**M2**
		t_{em}=5-50 (µm) $r_{em=}$ r_0/2 (max.)	**t_{em}=5-50 (µm) $r_{em=}$ r_0/2 (max.)**		**t_{em}=10-100 (µm) $r_{em=}$ r_0/2 (max.)**	**t_{em}=10-100 (µm) $r_{em=}$ r_0/2 (max.)**
300	161.63	155.15-102.87	149.5-39.7	20.20	19.39-12.86	18.7-5
500	1247.13	1197.12-793.76	1153.4-306.2	155.89	149.64-99.22	144.2-38.3
600	2586.05	2482.35-1645.94	2391.7-634.9	323.26	310.29-205.74	299-79.4
700	4790.98	4598.86-3049.32	4431-1176.1.	598.87	574.86-381.16	553.9-147

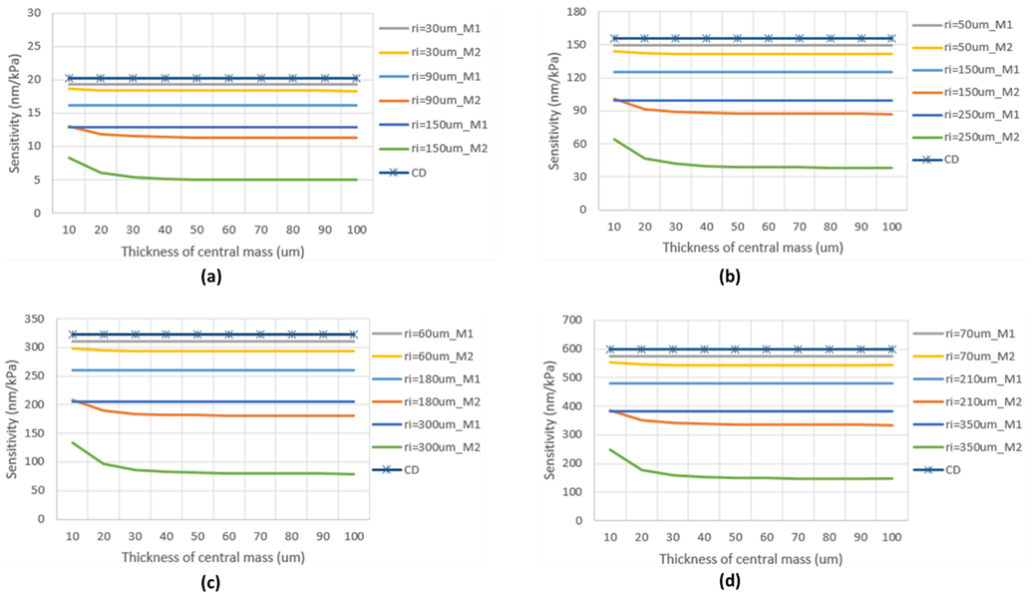

Figure 4 Comparison of diaphragm sensitivity (nm/kPa) considering the M1 model and M2 model. (a) t_m=10 µm and r_0=300 µm, (b) t_m=10 µm and r_0=500 µm, (c) t_m=10 µm and r_0=600 µm and (d) t_m=10 µm and r_0=700 µm

Moreover, sensitivity of diaphragm considering M1 model changes only with radius of embossment. This results can be explained when considering Eq.5-6. The narrower the width of embossment is, the larger the sensitivity. On the other hand, diaphragm sensitivity based on M2 model changes with both embossment thickness and radius. Analytical results of central displacement and sensitivity of diaphragm based on M2 model showed lower values compared to CD and M1 model based diaphragm. Sensitivity of M2 model based diaphragm is decreases, when the embossment thickness increases. Therefore, it was founded that sensitivity values of FPI diaphragm based on M1 and M2 models are not agrees well and there is discrepancy between these two models in terms of sensitivity. It is suggested that more experimental and numerical studies are required to find best model of embossment membrane and eliminate the differences between two models in terms of sensitivity.

4. CONCLUSION

The frequency response and sensitivity of MEMS based fiber optic pressure sensor diaphragm with a central embossment were analytically investigated and compared using two different models. These models were developed previously and available in literature [26,33]. As a result of these analyses, the following conclusions are reached. M1 model based diaphragm structure show better sensitivity than M2 model based diaphragm structure and however, this model ignores the effect of embossment thickness on sensor performance. From these results, differences between diaphragm sensitivities were calculated. For example, 149.64-99.22 nm/kPa and 144.2-38.3 nm/kPa sensitivity range were calculated for the diaphragm based on the M1 and M2 model, respectively when 500 μm in radius and 10 μm thick diaphragm was used for calculations. On the other hand, these two diaphragm model show very close frequency values. For example, frequency range of 600 μm in radius and 5 μm thick diaphragm was changes between 28.6-15.4 kHz and 28.7-15.4 kHz when M1 and M2 model was considered, respectively.

M2 model based diaphragm not only includes more geometrical parameters for determination of sensitivity and but also provides stiffer membrane compared to M1 model based diaphragm due to lower membrane deformation under same pressure conditions. This provides more flexibility to tune sensitivity response of sensor. From the point of view of frequency response, both of M1 and M2 model based diaphragm show slight differences between the fundamental frequencies for thinner and wider embossment.

As a conclusion, we hoped that the results obtained from this study will be used as a comparative study and help the obtain more accurate theoretical and practical models of embossed diaphragm for the future studies.

Acknowledgments

The authors would like to acknowledge the reviwers and editors of Sakarya University Journal of Science.

Funding

The author (s) has no received any financial support for the research, authorship or publication of this study.

The Declaration of Conflict of Interest/ Common Interest

No conflict of interest or common interest has been declared by the authors.

The Declaration of Ethics Committee Approval

This study does not require ethics committee permission or any special permission.

The Declaration of Research and Publication Ethics

The authors of the paper declare that they comply with the scientific, ethical and quotation rules of SAUJS in all processes of the paper and that they do not make any falsification on the data collected. In addition, they declare that Sakarya

University Journal of Science and its editorial board have no responsibility for any ethical violations that may be encountered, and that this study has not been evaluated in any academic publication environment other than Sakarya University Journal of Science.

REFERENCES

[1] A. P. Jathoul et al., "Deep in vivo photoacoustic imaging of mammalian tissues using a tyrosinase-based genetic reporter," Nat. Photonics, vol. 9, no. 4, pp. 239–246, 2015.

[2] J. Zhu, L. Ren, S. C. Ho, Z. Jia, and G. Song, "Gas pipeline leakage detection based on PZT sensors," Smart Mater. Struct., vol. 26, no. 2, 2017.

[3] X. Qi et al., "Fiber Optic Fabry-Perot Pressure Sensor with Embedded MEMS Micro-Cavity for Ultra-High Pressure Detection," J. Light. Technol., vol. 37, no. 11, pp. 2719–2725, 2019.

[4] H. F. Zhang, K. Maslov, G. Stoica, and L. V. Wang, "Functional photoacoustic microscopy for high-resolution and noninvasive in vivo imaging," Nat. Biotechnol., vol. 24, no. 7, pp. 848–851, 2006.

[5] W. Ni et al., "Ultrathin graphene diaphragm-based extrinsic Fabry-Perot interferometer for ultra-wideband fiber optic acoustic sensing," Opt. Express, vol. 26, no. 16, p. 20758, 2018.

[6] J. Liu et al., "Fiber-optic Fabry–Perot pressure sensor based on low-temperature co-fired ceramic technology for high-temperature applications," Appl. Opt., vol. 57, no. 15, p. 4211, 2018.

[7] B. Liang et al., "Highly Sensitive, Flexible MEMS Based Pressure Sensor with Photoresist Insulation Layer," Small, vol. 13, no. 44, pp. 1–7, 2017.

[8] I. Padron, A. T. Fiory, and N. M. Ravindra, "Modeling and design of an embossed diaphragm fabry-perot pressure Sensor," Mater. Sci. Technol. Conf. Exhib. MS T'08, vol. 2, no. October 2017, pp. 992–997, 2008.

[9] C. Liao et al., "Sub-micron silica diaphragm-based fiber-tip Fabry–Perot interferometer for pressure measurement," Opt. Lett., vol. 39, no. 10, p. 2827, 2014.

[10] Y. Zhang, L. Yuan, X. Lan, A. Kaur, J. Huang, and H. Xiao, "High-temperature fiber-optic Fabry–Perot interferometric pressure sensor fabricated by femtosecond laser," Opt. Lett., vol. 38, no. 22, p. 4609, 2013.

[11] F. Xu et al., "High-sensitivity Fabry–Perot interferometric pressure sensor based on a nanothick silver diaphragm," Opt. Lett., vol. 37, no. 2, p. 133, 2012.

[12] Z. Li et al., "Highly-sensitive gas pressure sensor using twin-core fiber based in-line Mach-Zehnder interferometer," Opt. Express, vol. 23, no. 5, p. 6673, 2015.

[13] S. J. Mihailov, D. Grobnic, C. W. Smelser, P. Lu, R. B. Walker, and H. Ding, "Bragg grating inscription in various optical fibers with femtosecond infrared lasers and a phase mask," Opt. Mater. Express, vol. 1, no. 4, p. 754, 2011.

[14] S. Liu et al., "Nano silica diaphragm in-fiber cavity for gas pressure measurement," Sci. Rep., vol. 7, no. 1, pp. 1–9, 2017.

[15] H. Y. Choi, G. Mudhana, K. S. Park, U.-C. Paek, and B. H. Lee, "Cross-talk free and ultra-compact fiber optic sensor for simultaneous measurement of temperature and refractive index," Opt. Express, vol. 18, no. 1, p. 141, 2010.

[16] M. Deng, T. Zhu, Y. J. Rao, and H. Li, "Miniaturized fiber-optic fabry-perot interferometer for highly sensitive refractive index measurement," 2008 1st

Asia-Pacific Opt. Fiber Sensors Conf. APOS 2008, vol. 16, no. 8, pp. 14123–14128, 2008.

[17] L. Zhang et al., "A diaphragm-free fiber Fabry-Perot gas pressure sensor," Rev. Sci. Instrum., vol. 90, no. 2, 2019.

[18] M. Nespereira, J. M. P. Coelho, and J. M. Rebordão, "A refractive index sensor based on a Fabry-Perot interferometer manufactured by NIR laser microdrilling and electric arc fusion," Photonics, vol. 6, no. 4, 2019.

[19] X. Wang et al., "Non-destructive residual pressure self-measurement method for the sensing chip of optical Fabry-Perot pressure sensor," Opt. Express, vol. 25, no. 25, p. 31937, 2017.

[20] J. Zhu, M. Wang, L. Chen, X. Ni, and H. Ni, "An optical fiber Fabry–Perot pressure sensor using corrugated diaphragm and angle polished fiber," Opt. Fiber Technol., vol. 34, no. 1, pp. 42–46, 2017.

[21] M. Manuvinakurake, U. Gandhi, M. Umapathy, and M. M. Nayak, "Bossed diaphragm coupled fixed guided beam structure for MEMS based piezoresistive pressure sensor," Sens. Rev., vol. 39, no. 4, pp. 586–597, 2019.

[22] X. Wang, B. Li, O. L. Russo, H. T. Roman, K. K. Chin, and K. R. Farmer, "Diaphragm design guidelines and an optical pressure sensor based on MEMS technique," Microelectronics J., vol. 37, no. 1, pp. 50–56, 2006.

[23] S. S. Kumar and B. D. Pant, "Polysilicon thin film piezoresistive pressure microsensor: design, fabrication and characterization," Microsyst. Technol., vol. 21, no. 9, pp. 1949–1958, 2015.

[24] B. Tian et al., "Fabrication and structural design of micro pressure sensors for Tire Pressure Measurement Systems (TPMS)," Sensors, vol. 9, no. 3, pp. 1382–1393, 2009.

[25] Z. Yu, Y. Zhao, L. Sun, B. Tian, and Z. Jiang, "Incorporation of beams into bossed diaphragm for a high sensitivity and overload micro pressure sensor," Rev. Sci. Instrum., vol. 84, no. 1, 2013.

[26] Y. Sun, G. Feng, G. Georgiou, E. Niver, K. Noe, and K. Chin, "Center embossed diaphragm design guidelines and Fabry-Perot diaphragm fiber optic sensor," Microelectronics J., vol. 39, no. 5, pp. 711–716, 2008.

[27] Z. Gong, K. Chen, Y. Yang, X. Zhou, and Q. Yu, "Photoacoustic spectroscopy based multi-gas detection using high-sensitivity fiber-optic low-frequency acoustic sensor," Sensors Actuators, B Chem., vol. 260, pp. 357–363, 2018.

[28] S. E. Hayber, T. E. Tabaru, and O. G. Saracoglu, "A novel approach based on simulation of tunable MEMS diaphragm for extrinsic Fabry–Perot sensors," Opt. Commun., vol. 430, no. August 2018, pp. 14–23, 2019.

[29] D. B. Duraibabu et al., "An optical fibre depth (pressure) sensor for remote operated vehicles in underwater applications," Sensors (Switzerland), vol. 17, no. 2, pp. 1–12, 2017.

[30] Z. Gong, K. Chen, Y. Yang, X. Zhou, W. Peng, and Q. Yu, "High-sensitivity fiber-optic acoustic sensor for photoacoustic spectroscopy based traces gas detection," Sensors Actuators, B Chem., vol. 247, pp. 290–295, 2017.

[31] C. Fu, W. Si, H. Li, D. Li, P. Yuan, and Y. Yu, "A novel high-performance beam-supported membrane structure with enhanced design flexibility for partial discharge detection," Sensors (Switzerland), vol. 17, no. 3, 2017.

[32] W. Ma, Y. Jiang, J. Hu, L. Jiang, and T. Zhang, "Microelectromechanical system-based, high-finesse, optical fiber Fabry–Perot interferometric pressure sensors,"

Sensors Actuators, A Phys., vol. 302, no. September, p. 111795, 2020.

[33] F. Wang, Z. Shao, J. Xie, Z. Hu, H. Luo, and Y. Hu, "Extrinsic fabry-pérot underwater acoustic sensor based on micromachined center-embossed diaphragm," J. Light. Technol., vol. 32, no. 23, pp. 4026–4034, 2014.

[34] Y. Yu et al., "Design of a Collapse-Mode CMUT with an Embossed Membrane for Improving Output Pressure," IEEE Trans. Ultrason. Ferroelectr. Freq. Control, vol. 63, no. 6, pp. 854–863, 2016.

[35] W. Zhang, H. Zhang, F. Du, J. Shi, S. Jin, and Z. Zeng, "Pull-In Analysis of the Flat Circular CMUT Cell Featuring Sealed Cavity," Math. Probl. Eng., vol. 2015, 2015.

[36] M. Chattopadhyay and D. Chowdhury, "Design and performance analysis of MEMS capacitive pressure sensor array for measurement of heart rate," Microsyst. Technol., vol. 23, no. 9, pp. 4203–4209, 2017.

[37] H. Gharaei and J. Koohsorkhi, "Design and characterization of high sensitive MEMS capacitive microphone with fungous coupled diaphragm structure," Microsyst. Technol., vol. 22, no. 2, pp. 401–411, 2016.

[38] J. Baltrušaitis, "Methylated Poly(ethylene)imine Modified Capacitive Micromachined Ultrasonic Transducer for Measurements of CO2 and SO2 in Their Mixtures," Sensors, vol. 19, no. 3236, 2019

[39] J. Ma, Miniature Fiber-Tip Fabry–Perot Interferometric Sensors for Pressure and Acoustic Detection (Doctoral dissertation), The Hong Kong Polytechnic University, 2014. http://hdl.handle.net/10397/7136.